







Beam and installation improvements of the NIO1 ion source

Cite as: Rev. Sci. Instrum. **91**, 013316 (2020); <https://doi.org/10.1063/1.5128658>

Submitted: 20 September 2019 . Accepted: 18 December 2019 . Published Online: 16 January 2020

M. Cavenago , M. Barbisan, R. Delogu, A. Pimazzoni, C. Poggi, M. Ugoletti, M. Agostini, V. Antoni, C. Baltador, V. Cervaro, M. De Muri , D. Giora, P. Jain, B. Laterza, G. Maero , M. Maniero, D. Martini, A. Minarello, D. Ravarotto, D. Recchia, A. Rizzolo, M. Romé , E. Sartori, M. Sattin, G. Serianni , F. Taccogna , V. Valentino, V. Variale, and P. Veltri



View Online



Export Citation



CrossMark



Lock-in Amplifiers

Zurich Instruments

Watch the Video

Beam and installation improvements of the NIO1 ion source

Cite as: Rev. Sci. Instrum. 91, 013316 (2020); doi: 10.1063/1.5128658

Submitted: 20 September 2019 • Accepted: 18 December 2019 •

Published Online: 16 January 2020



View Online



Export Citation



CrossMark

M. Cavenago,^{1,a)} M. Barbisan,² R. Delogu,² A. Pimazzoni,¹ C. Poggi,² M. Ugoletti,² M. Agostini,² V. Antoni,³ C. Baltador,¹ V. Cervaro,² M. De Muri,² D. Giora,¹ P. Jain,² B. Laterza,² G. Maero,⁴ M. Maniero,² D. Martini,¹ A. Minarello,¹ D. Ravarotto,² D. Recchia,² A. Rizzolo,² M. Romé,⁴ E. Sartori,² M. Sattin,¹ G. Serianni,² F. Taccogna,³ V. Valentino,⁵ V. Variale,⁵ and P. Veltri⁶

AFFILIATIONS

¹INFN-LNL, v.le dell'Università 2, 35020 Legnaro (PD), Italy

²Consorzio RFX, c. Stati Uniti 4, 35127 Padova, Italy

³CNR-Istituto Scienza e Tecnologia dei Plasmi, c. Stati Uniti 4, 35127 Padova, Italy

⁴Univ. Milano and INFN-MI, v. Celoria 16, 20133 Milano, Italy

⁵INFN-BA, v. Orabona 4, 70126 Bari, Italy

⁶ITER-Organization, 13067 St. Paul Lez Durance Cedex, France

Note: Contributed paper, published as part of the Proceedings of the 18th International Conference on Ion Sources, Lanzhou, China, September 2019.

^{a)} Author to whom correspondence should be addressed: cavenago@lnl.infn.it

ABSTRACT

The NIO1 (Negative Ion Optimization phase 1) source can provide continuous beam operation, which is convenient for systematic parameter and equipment studies. Even in the pure volume production regime, the source yield was found to depend on conditioning procedures. Magnetic configuration tests continued adding magnets to the existing setup; the filter field component B_x has been progressively extended to span the -12 to 5 mT range, and as a trend, source performances improved with $|B_x|$. The progress of camera beam diagnostics and of the quality of the volume-produced H^- beam is also shown. The status, off-line results, and reliability of a first NIO1 cesium oven are discussed; other upgrades in preparation (cavity ring down spectrometer, the end calorimeter, and conceptual tests of the energy recovery system) are also listed.

Published under license by AIP Publishing. <https://doi.org/10.1063/1.5128658>

I. INTRODUCTION

In view of the long term operation of neutral beam injectors (NBI) used for stellarator and tokamak heating and current drive,^{1,2} the negative ion source must be carefully optimized,³ especially because not only plasma but also surface wall conditions are involved in H^- or D^- production. The NIO1 source (Negative Ion Optimization phase 1, described elsewhere^{4,5}) was developed and has been operating since 2014 (in close collaboration between Consorzio RFX and INFN), as a convenient benchmark to study innovative solutions and to address physical questions. The comparatively smaller size of NIO1 (a compact 9 beamlet H^- source) is advantageous for experimental changes, whose significance is amplified by

the fact that NIO1 works in the Continuous Wave (CW) regime, as is necessary for DEMO.

As a first example of changes, several configurations (setups) of the source magnetic filter B^s were investigated (see Ref. 5); here, we add results obtained with the new setups “f2” and “f3” (described later). As another example, relations between source conditioning, evolution of H^- output, and radio frequency (rf) window cooling were noted and investigated. The paper is organized as follows: first, the overall plan of NIO1 is reviewed, describing a new beam camera diagnostics and remarkable conditioning procedures. Preparation of planned upgrades (cesium, cavity ring down, and calorimeter) is also reported. Second, the new filter field is discussed, highlighting the recent improvement in beam current.

II. OVERALL NIO1 PLAN, RESULTS AND UPGRADES

The NIO1 plasma chamber (a 0.21 m long cylinder with $R_c = 0.049$ m radius, see Fig. 1) has 9 extraction apertures (arranged in 3 rows and 3 columns with $L_x = 0.014$ m spacing), each with $R_h = 3.8$ mm radius, in the so-called plasma grid (PG), which is connected to a high voltage deck (HVD), held to potential $-V_s$ with respect to earth. The accelerator consists of 3 electrodes, namely, the extraction grid (EG) held to potential V_e with respect to the HVD and PG, the post acceleration (PA) grid connected to earth through an ammeter or a low voltage power supply, the repeller electrode (REP), followed by a 2-m long drift section made out of a pumping cross, a diagnostic tube, and an end flange (see Fig. 2), where a calorimeter with pepper pot holes is to be placed.

Strong permanent magnets (PMs) are embedded in the EG and the PA, giving a field B^d to deflect electrons out of the acceleration direction, which is our z axis. Let the x axis be aligned with these magnet longer sides;⁶ let $z = 0$ be the PG plane so that the source plasma region is $z < 0$ and the accelerator one is $z > 0$. Then, B^d is roughly aligned with the y -axis and negligible for $z \ll 0$. Let p_v be the pressure measured in the diagnostic tube and p_s the one in the source, the latter corrected for H_2 gas.

Up to now, the beam is intercepted by a fixed Carbon Fiber Composite (CFC) tile, similar to the spectral shear interferometry for direct electric field reconstruction (SPIDER) calorimeter,^{2,7} and biased to a voltage V_{cfc} in order to suppress secondary electron emission, hence collecting a nominal current signal I_{cfc} . The effect of V_{cfc} on I_{cfc} is well-known; at lower $V_{cfc} < 30$ V, the H^+ current is canceled by the electrons escaping the CFC, and at higher V_{cfc} , these e^- are attracted back to the CFC. However, the measurement is disturbed by the capture of other e^- produced by beam-gas collisions; up to now, we set $V_{cfc} \cong 60$ V as a compromise between these errors. We plan to transform this tile into a removable Faraday Cup (FC). A comparison with calorimetric CFC measurements of the beam current I_{cal} and power supply net current I_s^n (subtracting current into known resistances measured with plasma off) was done only in a few experiments, mostly at $V_s = 10.4$ kV, $V_s/V_e = 8$, depending on the infrared camera

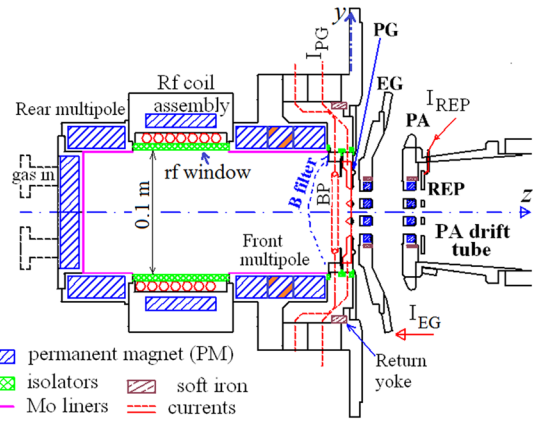


FIG. 1. Section zy of the NIO1 source with plasma grid PG and post extraction grid PA (see also the text).

availability; for a typical example, with $p_s = 0.75$ Pa, $p_v = 0.02$ Pa, and $I_{cfc} = 2.3$ mA, we got $I_{cal} = 1.7$ mA and $I_s^n = 3.4$ mA.

Even if NIO1 has no Faraday shield, the rf power P_k required to keep plasma on (level P_{k1}) or to keep inductive coupling (level P_{k2}) are similar in the case of hydrogen (say $P_{k1} \cong 0.8$ kW) so that capacitive coupling is rarely observed, as opposed to the oxygen case.⁸ Without plasma, the rf coil resonant frequency is 2.01 MHz with 140 Ω impedance. With hydrogen plasma and $P_k > 1$ kW, the rf can be set similarly (2.014 MHz mostly used) with no appreciable reflection for $p_s > 0.6$ Pa; this happens since enough plasma is generated to get a 50 Ω load, while at lower pressure ($p_s > 0.3$ Pa), reflection up to 5% can be observed.

Since the vessel gas pressure p_v typically ranges from about 0.2 Pa when only two turbopumps are used to 0.02 Pa when one cryopump is operated, beam stripping and ionization are not negligible, and light emission (mainly Balmer emission after beam-particle-gas collision) can be easily observed from television lateral cameras (TLCs) as TLC1 is toward the x direction and TLC2 is

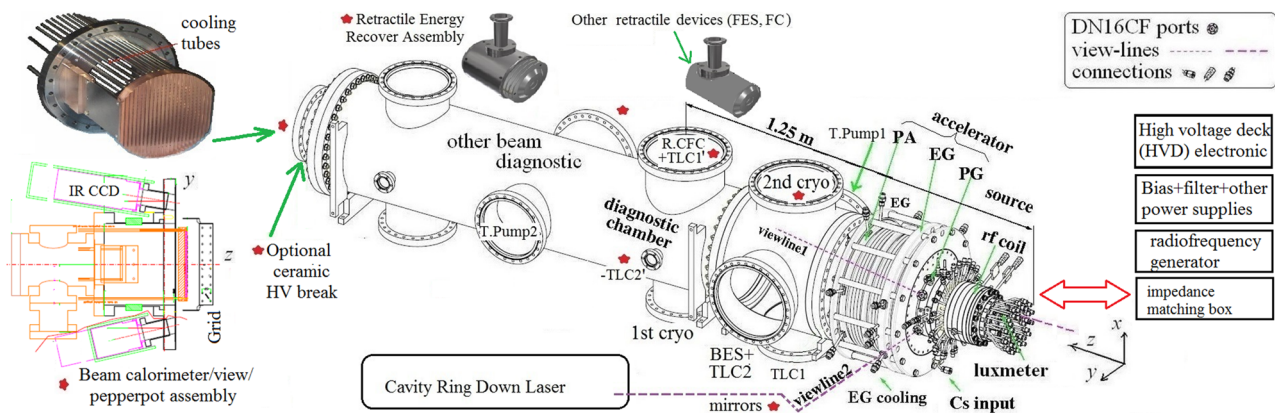


FIG. 2. NIO1 3D view including planned improvement ports (star markers), cameras (TLC), Faraday cup (FC), energy recover plugin, and end calorimeter with a possible new position of the infrared camera (IR CCD).

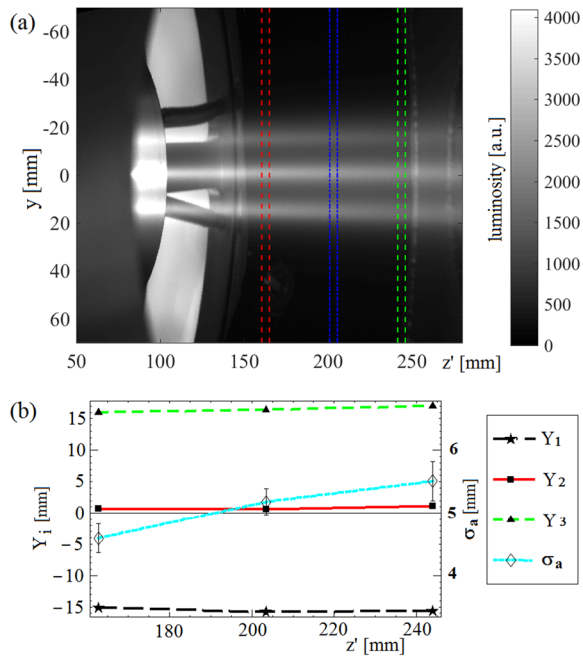


FIG. 3. (a) Image taken from monochrome camera TLC1 with 9 beamlets superposed into 3 columns (no perspective correction, coordinate refers to the median plane); note the three bands where the beam profile is sampled. (b) Fitted centroids Y_i of the beamlet columns (typical std error 0.5 mm, about marker size) and their rms width σ_a (average of the 3 columns).

toward the y direction. Beam profiles and beam divergences can thus be reconstructed⁹ (see Fig. 3); first, by averaging luminosity on a convenient z -interval, centered at $z' = z_1$, a luminosity profile $L(y)$ is obtained with 3 peaks due to the columns of beamlets, where $z' = z - z_R$ is a local coordinate with $z' \cong 0$ roughly being the repeller grid position; the column centroids Y_i and rms widths σ_i are obtained by a fit.⁹ The procedure is repeated for z_2 and z_3 , giving the result shown in Fig. 3(b), with σ_a being the average of σ_i . Then the widths are projected back to the repeller with linear fits,

$$Y_i(z_j) = \alpha_i + \beta_i z_j, \quad \sigma_i(z_j) = \gamma_i + d_i z_j, \quad (1)$$

where the fit parameters, α_i , β_i , γ_i , and the rms divergence d_i , depend on column index $i = 1, 2, 3$. More elaborate fits will require more data and hence, in practice, more cameras to cover a larger z span (we plan to put another camera TLC1' about 0.5 m downstream).

In the case shown, the initial centroids α_i are well compatible with the 14 mm spacing of grid holes, while rms divergence about 11 mrad (averaged on 3 columns) was a promising step toward a reasonable optics and needs better optimization as discussed later.

There are some specific features of NIO1 with respect to the SPIDER, which are briefly listed in this paragraph. In NIO1, an rf coil, accelerator insulators, and a Cs heater are in air, and the HVD is at PG potential (not at the EG one); the HV power supply stops at the first breakdown, which limits CW mode operation to $V_s < 25$ kV, also depending on the pressure and rf power used. No rf flip is observed, and no automatic capacitance tuning is installed. There is no Faraday shield.

The most striking feature of NIO1 may be related to the rf window. It was observed, in a true Cs-free operation, that the H^- current output benefits from large flows of air cooling of the rf window ($\cong 15$ m³/h at 2.5 absolute bar). Moreover, in 2019, the H^- current was increased (typically for half an order of magnitude) by one session of conditioning NIO1 with an oxygen plasma (a 5% mixing of Ar was added for enhancing visible emission); the effect persisted for some sessions but tended to decay after 3 sessions after which the conditioning session was repeated when possible. As a practical note on the present setup, sessions include about 4 h of continuous beam time, as limited by scheduling and preparation time, and changing gas requires one-day stops for installing or removing the O₂/Ar bottle and purging the NIO1 gas line. The installation of at least two auxiliary gas feeding points is well advanced.

Recognition of this O₂/Ar effect is related to the observation⁵ of the inverse correlation between I_{cfc} and the photomultiplier signal V_{pmt} (which measures plasma integrated luminosity) at constant control parameters, such as the pressure p_s , rf power p_k , and source voltages. A provisional heuristic interpretation is that a poor I_{cfc} is correlated with a somewhat larger electron temperature T_e in the rf driver, which explains the larger luminosity. The effectiveness of air cooling of the rf window indicates that the window status may significantly affect driver plasma. The oxygen conditioning was suggested by previous NIO1 operations,⁸ where oxygen was used as the main beam, with the deposition of films on the used rf window (some darkening was visible). To confirm the role of the rf window, the construction of a Faraday shield plug-in for NIO1 is being considered, which seems technically challenging for its reduced size. Even if the need for a more systematic investigation is clear (which will greatly benefit from a 160 mm internal diameter source NIO2 being promoted), the effect might open a new perspective on Cs-free negative ion sources in the continuous regime.

The NIO1 Cs oven was designed with a heat resistant valve to protect Cs during source ventilation; for further flexibility, an Ar purging line was added. The first method used to test the NIO1 Cs oven prototype (in a test bench completely separated from NIO1) was deposition on square Mo targets.⁵ As a second method, following the SPIDER oven experience,¹⁰ we installed a compact Surface Ionization Detector (SID)¹¹ in that test bench. Failure of a gate valve and frequent interruptions of main power caused air leaks and oxide crusts in the Cs reservoir, which was then rebuilt [see Fig. 4(a)]. Hence, Cs oven installation in NIO1 was rescheduled in Autumn. A preliminary calibration of the SID filament current I_f and its bias voltage V_1 measuring the emitted current I_1 was done; the filament voltage V_f is measured by a four-wire scheme, which allows the resistance to be measured (and average filament temperature T_{af} to be inferred) with 3.5 digit precision [see Fig. 4(b)]. Dark and dispersed current contribution I_d to I_1 changes appreciably during SID conditioning, and is not simply linear with V_1 [see Fig. 4(c)] (mainly due to the electronics used), while it does not appreciably increase with T_{af} . Current $I_f = 3.2$ A and voltage $V_1 = 60$ V were selected as the SID operation point, where the dark current $I_d \leq 90$ nA. New oven operation (for 8 h) up to a temperature of 130 °C showed some slow increase in I_1 to 120 nA, with the small value being mainly explained by the comparatively large distance between oven nozzle (2 mm radius) and SID filament (40 mm). From a preliminary calculation of Cs flow and tabulated vapor pressure, the efficiency of the Cs transfer pipe (held at 180 °C) is estimated to be about 10%.

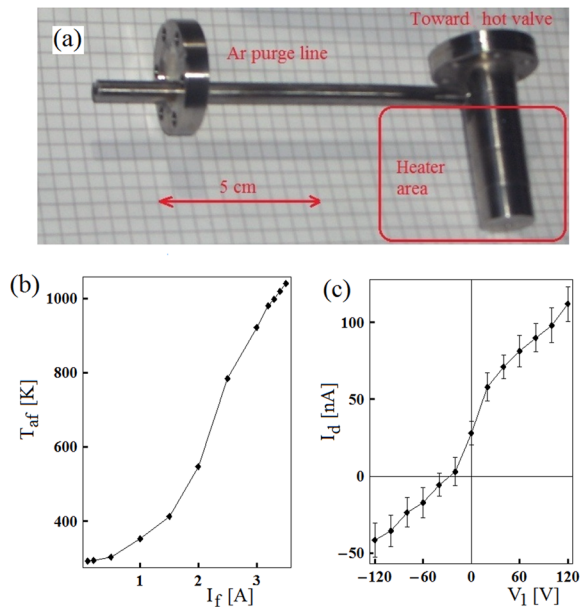


FIG. 4. (a) New Cs reservoir (with heater removed), (b) average filament temperature vs SID filament current I_f , and (c) preliminary data on dark and dispersed current I_d vs filament bias V_1 with respect to the chamber wall.

An important NIO1 upgrade is a compact Cavity Ring Down Spectrometer to measure H^- density (averaged along the line of sight), with two miniaturized shutters to protect mirrors from Cs when the laser is off; this is ready for installation on NIO1, with the exception of laser path protection cover, under construction.

The concept and plan of a beam energy recovery assembly (see Fig. 2) compatible with NIO1 are discussed elsewhere.¹² Another planned upgrade is the water-cooled calorimeter (with a CF200 flange, see Fig. 2) to be placed at the diagnostic tube end. While this calorimeter has a poor spatial resolution (7 mm), it is suited for measuring high power beams in the CW (without side diffusion of heat). Actually, the spatial resolution corresponds to an angular resolution of 3 mrad (and is well proportionate for a typical 10 mrad rms divergence). Moreover, a pepperpot emittance meter is easily integrated into this detector. The calorimeter will plug the z -axis viewport of the infrared camera, which will be moved to an angled viewport (9° with respect to the z -axis). This design also features calorimeter insulation from earth with a negatively biased suppressor grid before it; the grid may be a harp of thin wires (or a double harp) or a square mesh, whose shielding properties were calculated elsewhere.¹³ The suppression harp (or mesh) is a compromise between high transparency and good shielding and is convenient for Faraday Cups for large and perhaps unfocused beams.

III. NEW FILTER FIELD AND BEAM RESULTS

An H^- source needs a magnetic field B^s (called filter) inside the source near PG to protect fragile H^- from more energetic plasma electrons; the filter optimal value and profile are still debated.^{3,5}

In the original NIO1 configuration, called setup “a,” B^s was aligned in the x direction, to avoid interference with the deflection

field B^d , and was produced only by a current I_{pg} limited to 400 A; then, B_x^s had a modest maximum of 4 mT and an integral value of $\mathcal{I}_x = \int |B_x| = 0.08$ mT m. By adding external C-shaped conductors, in 2016, we built setup “b.” This gives $\mathcal{I}_x = 0.16$ mT m, which was very successful in enhancing O^- ion production.^{5,14} Let $\mathbf{B}^{(1)}$ be the field produced (by sole currents) in setup “b.” Setup “c” added a permanent magnet (PM) system producing a term $\mathbf{B}^{(2)}$ with a peak $B_y^{(2)} \cong 15$ mT, whose effectiveness was seemingly hindered by the interference with deflection field \mathbf{B}^d . In the setups “d” and “e,” the source field \mathbf{B}^s was left unchanged, but \mathbf{B}^d was changed (with new extraction grid magnets labeled EG3) to obtain cancellation of ion deflection in the acceleration.^{6,15} In setup “f,” we replace some source magnets with a new PM system, which produces a $\mathbf{B}^{(3)}$ term with peak $B_x^{(3)} = -5$ mT. As apparent from first experiments (end 2018), the beam was optimized by reversing I_{pg} (setup “f2”) so that $\mathbf{B}^{(1)}$ and $\mathbf{B}^{(3)}$ will reinforce each other (see Fig. 5). As a further test that a $|B_x|$ (or \mathcal{I}_x) increase is beneficial, we added some magnets also outside the source vacuum chamber, giving a term $B_x^{(4)}$ with a peak value of -4 mT. We call this setup “f3,” where $\mathbf{B}^s = -\mathbf{B}^{(1)} + \mathbf{B}^{(3)} + \mathbf{B}^{(4)}$. Since $B_x^{(1)}$ and $B_x^{(4)}$ are easily changed without opening the ion source, the filter field B_x^s now can span the $(-12, 5)$ mT range. As a trend, source performances improve with $|B_x|$, at least in NIO1 conditions (no cesiation, small radius R_c source): I_{cfc} is increased and the coextracted electron current is decreased by increasing I_{pg} and using the “f3” setup.

In Fig. 6, results for $|I_{cfc}|$ are shown, both with cryopump on (up to 7 mA) and off (up to 22 mA). On the other hand, it is well known that calorimetric currents I_{cal} are substantially lower, since secondary plasma can contribute to $|I_{cfc}|$. In the case of cryopump on, results roughly agree ($I_{cal}/|I_{cfc}| \cong 0.7$) so that the ion current at extraction may reach up to 20 A/m², which is typical of volume sources. In the case of cryopump off, the difference seems larger (even one order of magnitude) so that more accurate modeling and calibration are necessary.

The V_s/V_e voltage ratio was empirically adjusted (to about 9) for a better beam quality. In the case of Fig. 3, we had $V_s = 5.4$ kV and $V_e = 0.55$ kV with $I_{cfc} = -7.64$ mA, and in the source, $p_s = 0.9$ Pa, bias voltage $V_b = 35$ V, and bias plate current $I_{bp} = 0.3$ A. In the case

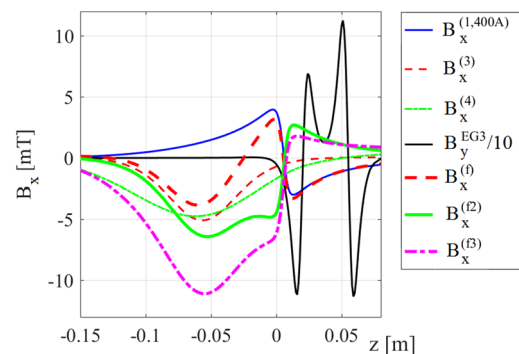


FIG. 5. Plot of B_x vs z . Setups “f,” “f2,” and “f3” are superpositions, defined in the text, of terms $B^{(1)}$ (here, at $I_{pg} = 400$ A), $B^{(3)}$, and $B^{(4)}$. For comparison, B_y from grid EG3 is shown (see the legend for scaling).

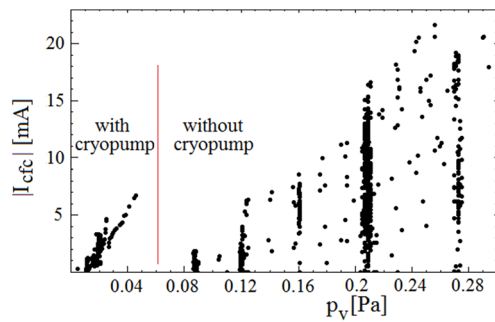


FIG. 6. Scatter plot of recent results for $|I_{cfc}|$ vs the vessel pressure p_v ; setup “f3.”

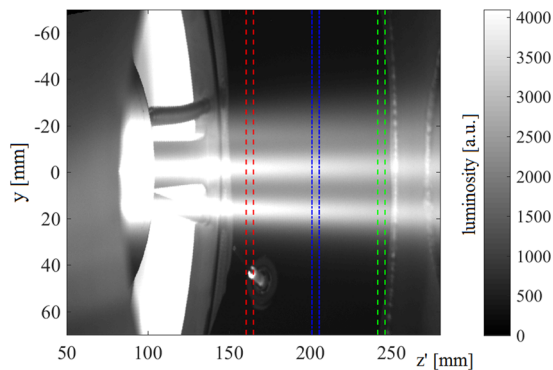


FIG. 7. Camera TLC1 with $V_s = 11.2$ kV and $V_e = 1.4$ kV.

of Fig. 7 with $V_s/V_e = 8$, the beam quality is lower also due to the larger current ($I_{cfc} = -20.5$ mA).

In Fig. 8(a) [with fixed $V_s = 9$ kV and V_e spanning the (0.6, 1.35) kV range], the central beamlet column divergence d_2 has a

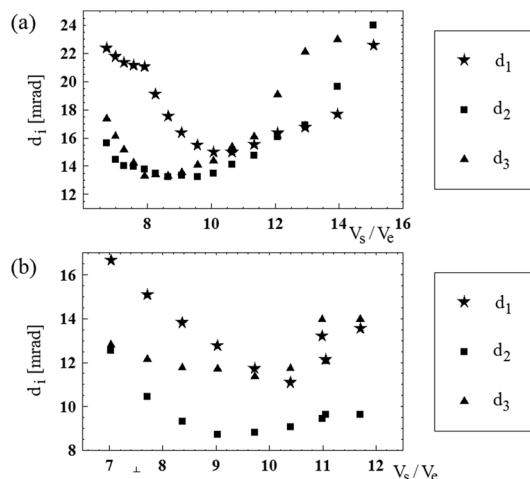


FIG. 8. (a) Beam column rms divergences d_i vs voltage ratio V_e/V_s with fixed $V_s = 9$ kV at $p_s = 0.75$ Pa; (b) same quantities but with fixed $V_e = 0.6$ kV at $p_s = 0.9$ Pa.

nice (wide) minimum around $V_s/V_e \cong 9$, while lateral ones d_1 and d_3 (affected by disuniformity of the filter field¹⁴ and plasma,⁵ and by viewing errors) suggest using a slightly larger $V_s/V_e \cong 9.5$. In Fig. 8(b), where $V_e = 0.6$ kV was held fixed, the d_2 optimal region (the minimum) is narrower but still around $V_s/V_e \cong 9$, and better beam optics are evident.

Since each calorimetric measurement I_{cal} requires a considerable time, we plan to improve I_{cfc} measurement with (1) independent voltages on repeller REP, grid PA, and CFC so that a positively biased repeller collects most of secondary electrons from gas ionization; (2) a change in the CFC geometry incorporating it into a Faraday cup (FC) with a proper suppressor; (3) making CFC removable, in order to avoid beam switch on/off.

The results of setup “f3” show both the advantage of operating at a larger filter field ($B_x \cong 12$ mT in the NIO1 geometry) and the importance of controlling all other side variables (rf window and conditioning). In conclusion, NIO1 operation has shown clear indications on the optimal filter direction and strength and on some effective beam diagnostics; of course, these are tailored to NIO1 specific conditions (CW operation, relatively small size of the plasma source). In Cs-free operation, conditioning with O_2 and/or increasing rf window cooling improves the H^- output. In parallel, after a commissioning of the Cs oven, some upgrading of the beam stop (water cooling) and high voltage system may be necessary for accommodating larger beam currents.

ACKNOWLEDGMENTS

Some parts of this research were financially supported by EUROfusion, commission INFN-5 (technological researches) or project INFN-E (energy).

REFERENCES

- H. Zohm, C. Angioni, E. Fable *et al.*, *Nucl. Fusion* **53**, 073019 (2013).
- V. Toigo, S. Dal Bello, E. Gaio *et al.*, *Nucl. Fusion* **57**, 086027 (2017).
- U. Fantz, P. Franzen, W. Kraus *et al.*, *Rev. Sci. Instrum.* **79**, 02A511 (2008).
- M. De Muri, M. Cavenago, G. Serianni *et al.*, *Fusion Eng. Des.* **96**, 249 (2015).
- M. Cavenago, G. Serianni, C. Baltador *et al.*, *AIP Conf. Proc.* **2052**, 040013 (2018).
- M. Cavenago and P. Veltri, *Plasma Sources Sci. Technol.* **23**, 065024 (2014).
- G. Serianni, M. De Muri, A. Muraro *et al.*, *Rev. Sci. Instrum.* **85**, 02A736 (2014).
- M. Cavenago, G. Serianni, M. De Muri *et al.*, *Rev. Sci. Instrum.* **87**, 02B320 (2016).
- M. Ugoletti, M. Agostini, M. Brombin, R. Pasqualotto, and G. Serianni, *Europhys. Conf. Abstr.* **43C**, P5.3012 (2019).
- A. Rizzolo, M. Barbisan, L. Bizzotto *et al.*, *Fusion Eng. Des.* **146**, 676 (2019).
- M. Fröschele, R. Riedl, H. Falter, R. Gutser, U. Fantz, and IPP NNBI team, *Fusion Eng. Des.* **84**, 788 (2009).
- V. Variale, M. Cavenago, P. Agostinetti, P. Sonato, and L. Zanotto, *Rev. Sci. Instrum.* **87**, 02B305 (2016).
- M. Cavenago, L. Bellan, and M. Comunian, *AIP Adv.* **8**, 125221 (2018).
- M. Cavenago, C. Baltador, and P. Veltri, *AIP Conf. Proc.* **2011**, 060003 (2018).
- G. Chitarin, P. Agostinetti, D. Aprile, N. Marconato, and P. Veltri, *Rev. Sci. Instrum.* **85**, 02B317 (2014).